



Green photoreduction synthesis of dispersible gold nanoparticles and their direct in situ assembling in multidimensional substrates for SERS detection

Zhengyi Chen¹ · Shengyong Lu² · Zhi Zhang² · Xuemei Huang¹ · Hao Zhao¹ · Jiaxin Wei¹ · Fengling Li¹ · Kunting Yuan³ · Linjing Su² · Yuhao Xiong²

Received: 22 August 2021 / Accepted: 26 June 2022 / Published online: 12 July 2022
© The Author(s), under exclusive licence to Springer-Verlag GmbH Austria, part of Springer Nature 2022

Abstract

Gold nanoparticles (AuNPs) and their composites have been applied in surface-enhanced Raman scattering (SERS) detection methods, owing to their stable and excellent surface plasmon resonance. Unfortunately, methods for synthesizing AuNPs often require harsh conditions and complicated external steps. Additionally, removing residual surfactants or unreacted reductants is critical for improving the sensitivity of SERS detection, especially when employing AuNPs-assembled multidimensional substrates. In this study, we propose a simple and green method for AuNPs synthesis via photoreduction, which does not require external surfactant additives or stabilizers. All the processes were completed within 20 min. Along this way, only methanol was employed as the electron acceptor. Based on this photoreduction synthesis strategy, AuNPs can be directly and circularly assembled in situ in multidimensional substrates for SERS detection. The removal of residual methanol was easy because of its low boiling point. This strategy was employed for the preparation of three different dimensional SERS substrates: filter paper@AuNPs, g-C₃N₄@AuNPs, and MIL-101(Cr)@AuNPs. The limit of detection of filter paper@AuNPs for thiabendazole SERS detection was 1.0×10^{-7} mol/L, while the limits of detection of g-C₃N₄@AuNPs and MIL-101(Cr)@AuNPs for malachite green SERS detection were both 5.0×10^{-11} mol/L. This strategy presents potential in AuNP doping materials and SERS detection.

Keywords Gold nanoparticles · Photoreduction synthesis · Green synthesis · Surface-enhanced Raman scattering · Multidimensional materials

Introduction

Gold nanoparticles (AuNPs) have received extensive attention in the field of surface-enhanced Raman spectroscopy (SERS) [1]. Their long-term stability [2], good biocompatibility [3], easily controllable size distribution [4], and fascinating optical properties [5] can efficiently scatter visible light and do not blink or photobleach. Importantly, AuNPs are endowed with the amplification of the Raman scattering efficiencies via their natural surface plasmon resonance, achieving analytes spectroscopic detection even at the single-molecule level [6], which results from electromagnetic and chemical enhancement mechanisms [7]. As the core of SERS, AuNPs can be obtained through many chemical methods [8], using different reducing agents such as sodium citrate, borohydrides, hydrogen peroxide, and stabilizing agents such as surfactants. However, these chemical methods have adverse effects on the environment and social health,

✉ Zhengyi Chen
chenzhengyi@glmc.edu.cn

✉ Linjing Su
linjingsu@163.com

✉ Yuhao Xiong
xiongyuhao@yeah.net

¹ Pharmacy School, Guilin Medical University, Guilin 541004, People's Republic of China

² College of Food and Bioengineering, Hezhou University, Hezhou 542899, People's Republic of China

³ Capital Construction Department, Guilin Medical University, Guilin 541004, People's Republic of China

owing to the application of toxic chemicals and solvents during synthesis.

Therefore, to overcome these limitations, green methods are being developed for AuNPs synthesis. These green methods usually employ plant extracts [9] or microorganisms [10, 11] as reducing and stabilizing agents. Although these biological syntheses of AuNPs offer significant benefits to the development of green chemistry, an in-depth understanding of the mechanisms underlying the biological synthesis of nanoparticles is challenging, and remains to be elucidated because of the complex compounds (with unknown structure, composition, concentration, and purity) [12]. Moreover, the size and shape of the AuNPs are not precisely controlled, and the particles may have poor chemical purity. Biomimetic synthesis [11] has become an attractive green strategy for AuNPs with well-defined size, shape, and chemical purity, as it uses specific biomolecules of known compositions, structures, and chemical properties, such as amino acids, peptides, proteins, nucleotides, and lipids. On the other hand, synthesis via laser ablation [13] or using solid reducing agents (e.g., stainless steel [14]) provide feasible strategies to solve the poor chemical purity problems during AuNPs producing because they does not require a stabilizing agent.

Despite these substantial achievements, a few issues still need to be addressed for SERS detection using AuNPs. Generally, the residual reducing agents or stabilizing agents absorbing on the AuNPs should be removed before SERS detection, because the Raman intensity of the molecules can significantly amplify when they are placed in close proximity of the hot spots of AuNPs (< 1 nm) [15]. For example, citrate is a frequently used reducing and stabilizing agents for chemical synthesis of AuNPs, and its influence for SERS detection was deeply investigated by the group of Prof. Karen Johnston [16]. Therefore, removing the surfactant from the surface of AuNPs becomes necessary before SERS detection or modification [17]. These procedures are labor-intensive, and can easily cause the AuNPs to aggregate. Additionally, assembling AuNPs in multidimensional materials has been a concern, because the sensitivity and stability of SERS detection can be significantly improved by fixing the hot spots in an ordered regular arrangement on a large surface [18]. Many multidimensional materials are available for SERS substrates, such as cellulose paper (one dimension) [15], graphene (two dimensions) [19], and MOFs (three dimensions) [20]. In order to assemble AuNPs in multidimensional materials, many methods have been developed, such as in situ chemical reduction and self-assembling [20]. In these ways, the surfactants or unreacted reductants would be trapped into the pores of the multidimensional materials, resulting in poor Raman enhancement ability because of the loss of hot spots. In this status, removing the residual surfactants or unreacted reductants became necessary but it

seemed difficult because of their high surface area of multidimensional materials. Therefore, for AuNP synthesis, it is challenging to develop a strategy that allows their efficient assembly in multidimensional materials without surfactants and removes the unreacted reductants easily.

The photoreduction of metal precursors on different surfaces has been widely studied, owing to its advantages of not requiring harmful and strong reducing agents, possible room-temperature operation, and noninvasive and immediate acting features of light [21–23]. Unfortunately, most of the photoreduction to create AuNPs unavoidably employed reducing agents or surfactants, such as polypeptide copolymer [23] and polyoxyethylene 4-lauryl ether [24], which are difficult to remove and unfavorable for assembling AuNPs in multidimensional materials. Marek Wojnicki's group reported the tetrachloroaurate acid could be photo-reduced by methanol [25]. Although they did not find AuNPs formation in their experiments, it inspired us to continue to use methanol for AuNPs synthesis because methanol could not be absorbed in multidimensional materials and easily washed. In this work, we propose a green strategy based on photoreduction for AuNPs synthesis without surfactants, which was employed for direct in situ assembling of AuNPs in multidimensional substrates for SERS. To demonstrate the feasibility of these SERS substrates, they are employed for the SERS analysis of malachite green and thiabendazole.

Experimental

Materials and instruments

Chloroauric acid ($\text{HAuCl}_4 \cdot 4\text{H}_2\text{O}$, 99.9%), malachite green (MG), and thiabendazole (TBA) were purchased from Beijing HWRK Chemical Co., Ltd. (Beijing, China). Methanol (high-performance liquid chromatography (HPLC) grade), ethanol, isopropyl alcohol, and N-butyl alcohol were purchased from Sigma-Aldrich (Shanghai, China). Melamine, terephthalic acid, $\text{Cr}(\text{NO}_3)_3 \cdot 9\text{H}_2\text{O}$, hydrofluoric acid, NaCl, and 2,4-dinitrophenylhydrazine were purchased from Macklin Biochemical Co., Ltd. (Shanghai, China). UV–vis absorption spectra were recorded on a Cary 60 spectrophotometer (Agilent, USA). Raman measurements were performed using a Thermo Fisher DXR Raman spectrometer that was equipped with a standard 632.8 nm HeNe 10 mW laser and CCD detector (Thermo, USA). Transmission electron microscopy (TEM) images were obtained using an FEI TECNAI G20 instrument (FEI, USA). Dynamic light scattering (DLS) measurements were performed using a NanoZS90 (Malvern, UK) instrument. HPLC measurements were performed using a Waters Acquity H-CLASS (Waters, USA). Powder X-ray diffraction patterns were obtained using a D/max 2550 VB/PC diffractometer (Rigaku, Japan).

Water samples were from the fishpond in local. Apples are bought from local market.

Synthesis of pure AuNPs in solution

In a quartz bottle, 2.0 mL of 0.2 g/L HAuCl_4 solution was mixed with 2.0 mL of 40% methanol solution. Subsequently, this solution was irradiated with a 70-W UV lamp (365 nm) for 15 min. The obtained purple AuNP solution was stored in a refrigerator at 4 °C.

In situ assembling of AuNPs on filter paper

The well-cut filter paper ($W \times L = 15 \times 35$ mm) was loaded vertically into a quartz bottle. Subsequently, 2.0 mL of 40% methanol solution and 2.0 mL of different concentrations of HAuCl_4 solution (0.2, 0.4, 0.6, 0.8, 1.0 g/L) were added and mixed. The mixed solution in the quartz bottle was irradiated with a 70-W UV lamp for 20 min. Finally, the AuNP-loaded filter paper was removed, washed with deionized water several times, and allowed to air dry.

Synthesis of g- C_3N_4 @AuNPs

The bulk g- C_3N_4 was synthesized by the pyrolysis of melamine, following previous procedures with some modifications [26]. Briefly, 15 g of melamine was placed in a crucible and heated at 550 °C in a furnace for 3 h (temperature ramp of 5 °C min^{-1}). After cooling to room temperature naturally, a light-yellow bulk of g- C_3N_4 was obtained. To obtain the g- C_3N_4 nanosheets, 0.5 g of bulk g- C_3N_4 powder was dispersed in 25 mL methanol. Subsequently, the mixed solution was probe-sonicated (Ultrasonic Processor KQ-400KDV) for 150 min at 380 W. The g- C_3N_4 nanosheet supernatant, with a high concentration, was collected using centrifugal separation, and stored in a refrigerator at 4 °C.

In a quartz bottle, 2.0 mL of g- C_3N_4 nanosheet methanol supernatant and 2.0 mL of 1.0 g/L HAuCl_4 solution were mixed. Subsequently, the mixed solution was irradiated with a 70 W UV lamp for 25 min. Finally, the resulting solution was centrifuged at 11,000 rpm for 10 min. The precipitated g- C_3N_4 @AuNPs were washed three times with deionized water, re-dispersed in water, and stored in a refrigerator at 4 °C.

Synthesis of MIL-101(Cr)@AuNPs

MIL-101(Cr) was synthesized according to our previous work [27], with some modifications. Briefly, 800 mg of $\text{Cr}(\text{NO}_3)_3 \cdot 9\text{H}_2\text{O}$, 332 mg of terephthalic acid, and 0.1 mL of hydrofluoric acid were mixed well with 9.6 mL deionized water in a teflon-lined bomb, and subsequently, reacted in an oven and heated at 220 °C for 8 h. The

precipitated MIL-101(Cr) was collected using centrifuge separation, and washed five times with ethanol and deionized water. Finally, the samples were dried overnight at 150 °C in vacuo.

In a quartz bottle, 5.0 mg of MIL-101(Cr) dispersed in 20 mL of 40% methanol solution was mixed with 2.0 mL of 1.0 g/L HAuCl_4 solution. Subsequently, the mixed solution was irradiated with a 70 W UV lamp for 90 min. The resulting solution was centrifuged at 11,000 rpm for 5 min, and the precipitated MIL-101(Cr) @AuNPs were washed three times with deionized water, re-dispersed in water, and stored in a refrigerator at 4 °C.

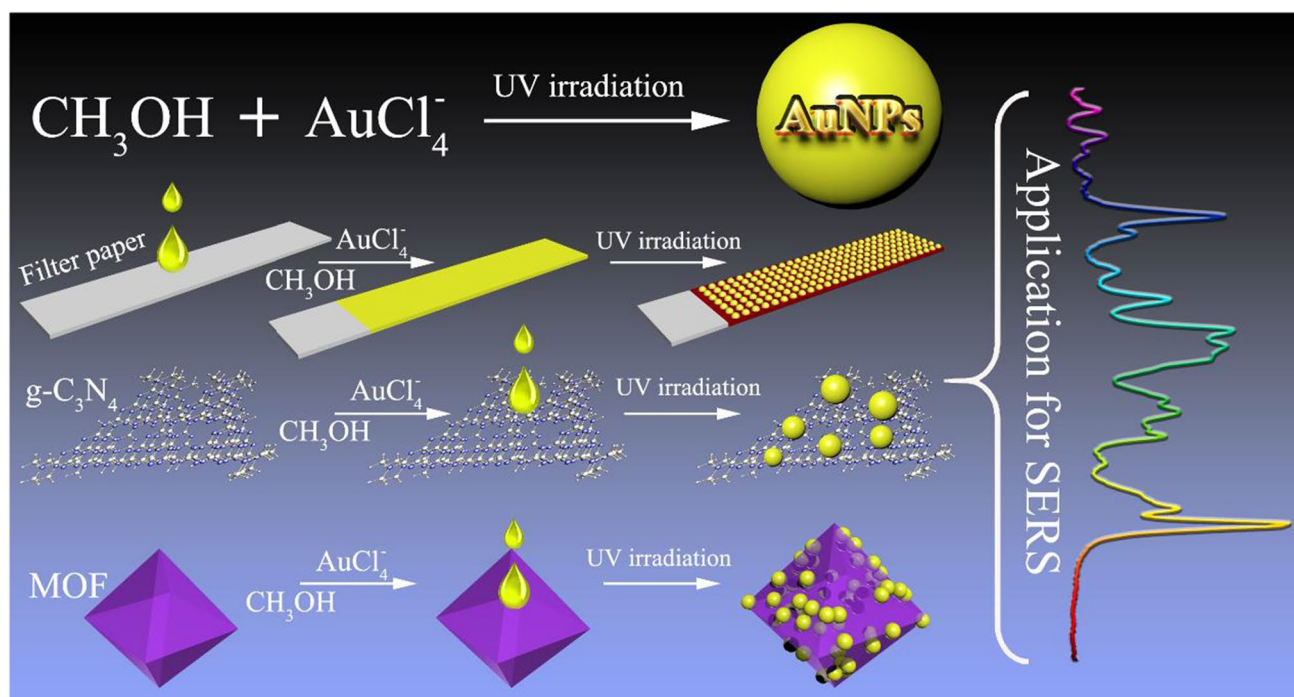
Determination of formaldehyde via HPLC method

The formaldehyde, which was generated from methanol during the photochemical synthesis of AuNPs, was analyzed using HPLC. Briefly, 1.0 mL of freshly synthesized AuNPs was centrifuged at 11,000 rpm for 15 min. Subsequently, 100 μL of the supernatant was removed using a pipette, and immediately mixed with 400 μL of deionized water and 400 μL of 2.0 mg/mL 2,4-dinitrophenylhydrazine acetonitrile solution. The solution was incubated for 30 min at 70 °C. After the reaction, the solution was filtered through a 0.25- μm nylon membrane filter, and analyzed immediately using HPLC. Conditions were as follows.

The column was Shim-pack GIST C18 [2.1 mm (i.d.) \times 100 mm (L), 3 μm], which was produced from Shimadzu company (Japan). The mobile phase consisted of 0.1% trifluoroacetic acid aqueous solution (solvent A) and acetonitrile (solvent B). The mobile phases were eluted at 0.5 mL/min at 40 °C with the gradient as follows: 30% B at beginning was kept in 0.50 min and then linear ascended to 80% within 4.50 min and held for 1.0 min, then decreased to 30% within 0.50 min and held for 2.50 min. The wavelength of UV detector was set at 355 nm.

SERS determination of MG by homogeneous AuNPs, g- C_3N_4 @AuNPs, and MIL-101(Cr)@AuNPs active substrates

1.0 mL of serial concentration of 0.05×10^{-7} – 1.64×10^{-7} mol/L MG solution was mixed well with 120 μL of AuNPs, and then, 50 μL of 10 mg/L NaCl solution was added. For g- C_3N_4 @AuNPs, and MIL-101(Cr)@AuNPs, 1.0×10^{-10} mol/L MG solution was mixed well with them. After 2 min, the mixture was measured using a Raman spectrometer over the spectral response range of 500–3000 cm^{-1} , with a laser wavelength of 633 nm, power of 3 mW, and acquisition time of 10 s. Centrifugal treatment was for fishpond water at 8000 r/min. And then, AuNPs, g- C_3N_4 @AuNPs, and MIL-101(Cr)@AuNPs for SER detection of MG in the supernatant were as the same of MG standard solution.



Scheme 1 Process of photoreduction synthesis of dispersible AuNPs and direct in situ assembly in multidimensional substrates

SERS determination of MG and TBA by AuNPs loaded filter paper

A piece of AuNPs-loaded filter paper was prepared, and a circle with a diameter of 5 mm was drawn using a hydrophobic pen. Subsequently, 50 μL of MG solution was dropped on the circle, and allowed to air dry. The dropped-air dried sequence was repeated five times. 10 μL of TBA solution was spread onto the surface of apple peel (about 1 cm^2). When the solvent was evaporated, 10 μL of methanol was dropped onto apple surface. Then, the prepared filter paper@AuNPs were entirely attached to the apple surface. When the filter paper@AuNPs was applied to swab apple peel, a certain pressure (about 2 N) was kept by making the reading on a scale of filter paper@AuNPs. After swabbing, the filter paper@AuNPs were for further SERS analysis. The MG and TBA containing AuNP-loaded filter paper was measured using a Raman spectrometer over the spectral response range of 500–3000 cm^{-1} , with a laser wavelength of 633 nm, power of 3 mW, and acquisition time of 10 s.

Results and discussion

Strategy

The process of photoreduction synthesis of dispersible gold nanoparticles and their direct in situ assembling in

multidimensional substrates for SERS detection were illustrated in Scheme 1. The AuNPs were synthesized through the photoreduction of AuCl_4^- by methanol, which acted as an electron acceptor. The entire process was performed in minutes rather than hours, under mild conditions, without using any stabilizing ligands containing S, N, and P, which are considered necessary for conventional synthetic approaches of AuNPs [28]. Furthermore, AuNPs were easily assembled in multidimensional materials via this strategy, and removing residual methanol was easier than removing other reductants. To demonstrate this method for multidimensional substrate synthesis, filter paper, $\text{g-C}_3\text{N}_4$, and MIL-101(Cr) were employed as one-dimensional, two-dimensional, and three-dimensional materials, respectively. And their application for SERS were investigated by MG or TBA, which were the widely concerned targets in environment and food safety. The details associated with each step of this study are as follows.

Characterization and application for SERS

Figure 1A exhibits the typical localized surface plasmon resonance (LSPR) band of AuNPs at 530 nm after 3 min of irradiation. Notably, longer wavelength absorption at $\lambda > 600$ nm appeared after 15 min of irradiation. It was assigned to interparticle plasmon excitons of AuNP multimers or other shape of AuNPs (rods, hexagonal, or triangular) [29], which were observed using transmission

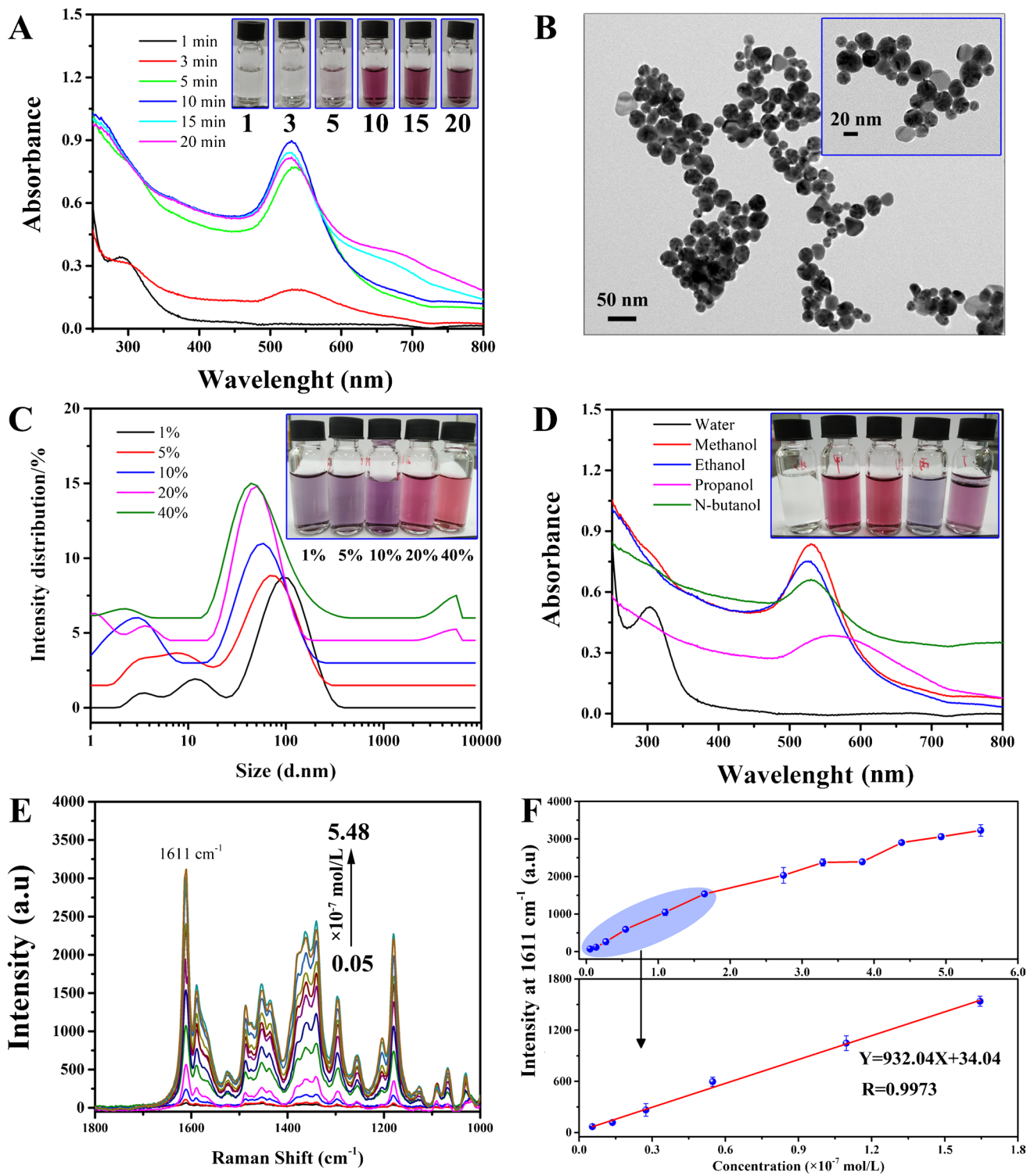


Fig. 1 Characterization of photoreduction synthesis of AuNPs and its application for SERS detection. **A** UV–vis spectra of AuNPs as a function of ultraviolet irradiation time. Inset: Corresponding photographs. **B** TEM of AuNPs. Condition: 40% methanol (v/v), 15 min.

DLS measurements of the effects of methanol concentration (**C**) and alcohols (**D**) on AuNPs. Inset: Corresponding photographs. **E** SERS spectra of different concentrations of MG. **F** Linear scale of MG at 1611 cm^{-1} of Raman shift

electron microscopy (TEM) (Fig. 1B; Fig. S1) This suggested that the complexity of the formed AuNPs occurred after 15 min of irradiation. This result agreed with the dynamic light scattering (DLS) data (Fig. S2), exhibiting bimodal distribution of AuNPs, which confirmed the existence of other shapes of AuNPs. As shown in Fig. 1B, the TEM observations of the AuNPs, which were obtained after 15 min of irradiation, confirmed the formation of AuNPs with an average diameter of approximately 35 ± 2.0 nm, ranging from 10 to 40 nm. However, the AuNPs were well dispersed in the solution, as confirmed by the photographs in Fig. 1A. Notably, an interesting phenomenon was observed on careful comparison of the UV scan curves between 3 and 5 min. The absorbance increased significantly; therefore, a careful UV scanning was conducted at 0.5-min intervals of irradiation. The results (as illustrated in Fig. S3) demonstrate that the shape of the UV scan curves became consistent after 5.5 min of irradiation (Fig. S3A), and that the absorbance change rate at 4.5 min of irradiation was the fastest (Fig. S3B). This phenomenon was different from the other AuNPs preparations via UV methods [30, 31]. We speculated that it was because of the autocatalytic surface growth mechanism of AuNPs (formation of Au nuclei and catalytic $[\text{AuCl}_4]^{2-}$ reduction on the surface, which was followed by Au deposition) [32] and the electron acceptor agent of CH_3OH without UV absorption.

A schematic of the probable mechanism of AuNPs formation, using CH_3OH as the electron acceptor, is depicted in Fig. S4. The initial photochemical step by excitation of $[\text{AuCl}_4]^-$ species involved electron transfer from Cl^- to the metal center owing to the ligand-to-metal charge transfer of the absorption bands, generating Cl^\cdot radicals and $[\text{AuCl}_4]^{2-}$ intermediate species [33]. Subsequently, the Cl^\cdot radicals interacted with methanol via hydrogen abstraction to form hydroxymethyl radicals ($\dot{\text{C}}\text{H}_2\text{OH}$) (reaction 1). These radicals exhibited high reducing ability and participated in the reduction of $[\text{AuCl}_4]^-$ species, to yield formaldehyde (HCHO) (reaction 2). Contrarily, the $[\text{AuCl}_4]^{2-}$ ions were unstable and transformed into more stable $[\text{AuCl}_2]^-$ and $[\text{AuCl}_4]^-$ ions via a fast disproportionation reaction (reaction 3). Subsequently, $[\text{AuCl}_2]^-$ was combined with $[\text{AuCl}_4]^{2-}$ species through a disproportionation reaction, to generate Au^0 (reaction 4). Finally, many Au^0 nuclei were formed and grew into AuNPs (reaction 5). The methanol behaved as a sacrificial agent to trap photogenerated electrons, and was oxidized to HCHO (reaction 6). HPLC was used for the quantitative analysis of the HCHO generated in reactions 2 and 6 (Fig. S5A, B). As shown in Fig. S5C, a characteristic peak of the HCHO derivative was observed,

and its signal increased with the increase in irradiation time. This indicated the oxidation of CH_3OH into HCHO in the irradiation synthesis pathway. This photoreduction of tetrachloroaurate acid by methanol resulting in HCHO was reported by Marek Wojnicki's work [25]. Importantly, these results confirmed that AuNPs were mainly formed via the autocatalytic mechanism. As shown in Fig. S5D, the profile for HCHO formation agreed with the increased LSPR absorbance profile (Fig. S3B), where the HCHO formation was accelerated by the formation of AuNPs. This indicated the acceleration in the photoreduction of $[\text{AuCl}_4]^-$ (reaction 2, Fig. S4) on the surface, owing to the local heating of the AuNP surface via light absorption [34]. This allowed smooth Au deposition on the surface and led to AuNPs growth.

Figure 1C exhibits the effects of the amount of CH_3OH on the DLS of the AuNPs. The average diameter of the AuNPs decreased with the increase in the amount of CH_3OH , because it created numerous $[\text{AuCl}_4]^{2-}$ and produced several Au^0 nuclei. The inset photographs in Fig. 1C illustrates the blue shift of LSPR with an increase in the amount of CH_3OH , which was caused by the triangular and hexagonal large Au plates with (111) planes formed in the presence of a low amount of CH_3OH . Figure 1D demonstrates that other alcohols can also be employed as reductants for the photoreduction synthesis of AuNPs, such as ethanol, propanol, and N-butanol. However, a red shift of LSPR occurred on employing long-chain alcohols, such as propanol and N-butanol (as shown in the photographs in Fig. 1D). This suggested that the synthesis of AuNPs via the proposed strategy could be controlled by the amount and type of alcohol used

Before application for SERS analysis, the stability of AuNPs preparation was confirmed under the condition of 40% CH_3OH and 15 min of irradiation (Fig. S6). Subsequently, the AuNPs were employed as the SERS substrate for detecting malachite green (MG), which was related to the safety of aquatic lifeforms. On the other hand, the addition of NaCl was necessary because it made the AuNPs and the analytes aggregated together, resulting in the improving SERS signal via "hot spot" formation [35]. Therefore, the investigation of NaCl concentration was carried out. Figs. S7 and S8 show that the SERS signal of MG increased with the increasing concentration of NaCl in the range of 1 to 10 mg/L but decreased when increasing to 20 mg/L. The reason might be the excessive aggregation of AuNPs, which were confirmed by the UV spectrum (Fig. S9). After obtaining the optimizing the concentration of NaCl (10 mg/L), quantitative SERS detection was achieved by changing the MG concentration. As shown in Fig. 1E, the SERS

signal of the MG steadily increased with the increasing MG concentration. The intensity of the strongest peak at 1611 cm^{-1} was used for the quantitative evaluation of MG. A good linear relationship was observed in the range of 0.05×10^{-7} – 1.64×10^{-7} mol/L with a correlation coefficient of 0.9973 (Fig. 1F). The limit of detection was 0.02×10^{-7} mol/L with a signal-to-noise ratio of 3. These results demonstrated the excellent SERS activity and ability of quantitative analysis of the synthesized AuNPs.

Filter paper@AuNPs for SERS

The paper-based SERS substrates have been highlighted as versatile green platforms, owing to their weak SERS response, flexibility, and portability, and have been widely used in real-time detection [36, 37]. Figure 2 illustrates the proposed strategy of photoreduction synthesis of AuNPs assembled in situ on filter paper for SERS detection. Figure 2A indicates that the color of the filter paper deepens with an increase in the concentration of $[\text{AuCl}_4]^-$, suggesting the assembling of more AuNPs on it. The amount of AuNPs could be controlled by the concentration of $[\text{AuCl}_4]^-$ (Fig. 2A) as well as the growth time, as shown in Fig. 2B. The TEM images illustrate the deposition of AuNPs on the filter paper (Fig. 2C). Figure 2D indicates that when filter paper@AuNPs was used, the SERS signal of MG (1.0×10^{-8} mol/L) was dramatically stronger than that (1.6×10^{-7} mol/L MG) of the AuNPs at 1611 cm^{-1} of

Raman shift, suggesting the sample concentration property of the filter paper. On the other hand, the flexibility of filter paper@AuNPs suits to the in situ SERS detection [38] via swabbing the surface of sample, such as fruits. Therefore, the obtained filter paper@AuNPs were employed for SERS detection of pesticide residues on the surface of apples. Considering thiabendazole (TBA) was a typical pesticide which has been widely used; we chose TBA as the analyte to check up the feasibility and validity of filter paper@AuNPs. Fig. S10 A shows that the SERS signal of the TBA steadily increased with its increasing concentration. The intensity of the strongest peak at 1594 cm^{-1} was used for the quantitative evaluation of TBA. A good linear relationship was observed in the range of 3.0×10^{-7} – 18.0×10^{-7} mol/L with a correlation coefficient of 0.9930 (Fig. S10B). The limit of detection was 1.0×10^{-7} mol/L with a signal-to-noise ratio of 3.

g-C₃N₄@AuNPs for SERS

Recently, noble metal growth on 2D nanomaterials has been studied extensively, owing to their unique properties and various applications in electronics, catalysis, energy storage devices, and SERS [39]. The growth method of noble metals on 2D materials in solution is more advantageous than the traditional vapor-phase deposition method because of its low throughput and high cost, arising from the requirement of ultra-high vacuum conditions and special equipment [40]. Figure 3 illustrates the proposed strategy for the

Fig. 2 In situ assembling of AuNPs on filter paper and its application for SERS detection. **A** Photographs of in situ assembling of AuNPs on filter paper with various concentrations of HAuCl_4 . **B** Photographs of multiple growths of AuNPs on filter paper. **C** TEM of AuNPs assembled on filter paper. **D** SERS detection of MG with the filter paper@AuNPs. 1.6×10^{-7} mol/L MG for AuNPs; 1.0×10^{-8} mol/L of MG for paper@AuNPs

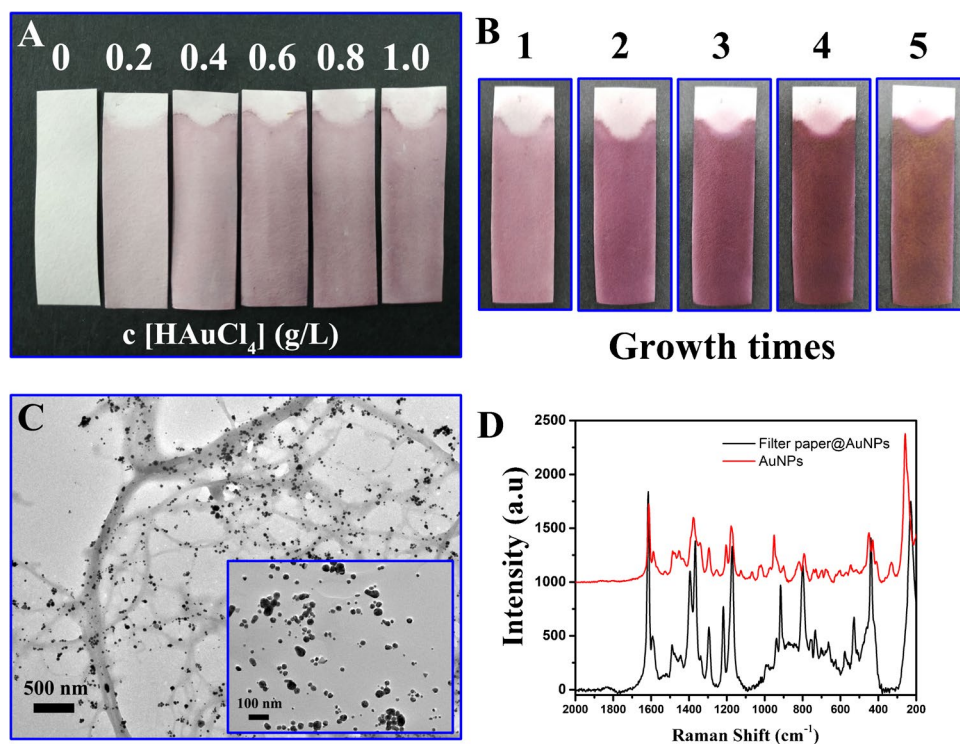
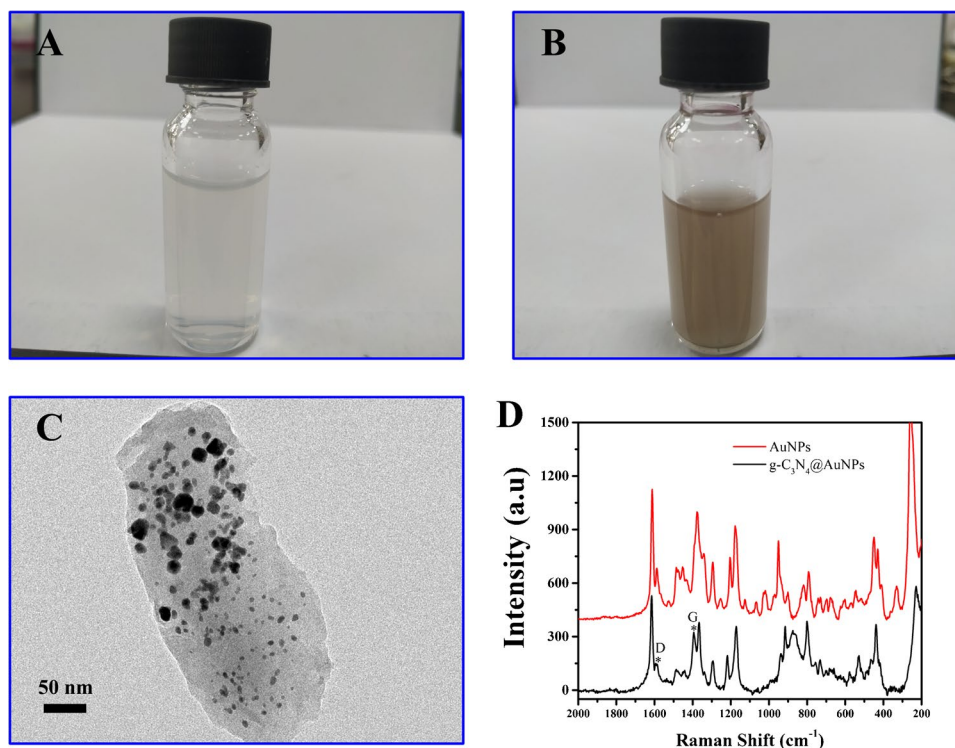


Fig. 3 In situ assembling of AuNPs in g-C₃N₄ and its application for SERS detection. **A** Photographs of g-C₃N₄ aqueous solution. **B** Photographs of g-C₃N₄@AuNPs aqueous solution. **C** TEM images of g-C₃N₄@AuNPs. **D** SERS detection of MG with g-C₃N₄@AuNPs. 1.6×10^{-7} mol/L of MG for AuNPs; 1.0×10^{-10} mol/L of MG for g-C₃N₄@AuNPs



in situ assembly of AuNPs in g-C₃N₄ for SERS detection. Figure 3A and B illustrate that the g-C₃N₄@AuNPs were well dispersed and the color of the g-C₃N₄ aqueous solution turned brown (red shift) after AuNPs assembly. This suggests that the g-C₃N₄@AuNPs were successfully prepared, as verified by TEM (Fig. 3C). Figure 3D illustrates that the Raman shift of MG from g-C₃N₄@AuNPs corresponded to that of the AuNPs, except the peak at 1592 cm⁻¹ and 1394 cm⁻¹, corresponding to the D-band and G-band of g-C₃N₄ [42].[41] However, the SERS signal of MG (1.0×10^{-10} mol/L) was dramatically stronger than that (1.6×10^{-7} mol/L MG) of the AuNPs at 1611 cm⁻¹ of Raman shift, owing to the enrichment ability of the g-C₃N₄ and the 3D hot spots [42]. Fig. S11 A compares the SERS signal of the same concentration MG obtained from g-C₃N₄@AuNPs and AuNPs. The SERS signal of MG from g-C₃N₄@AuNPs was about 62-fold as high as AuNPs.

MIL-101(Cr)@AuNPs for SERS

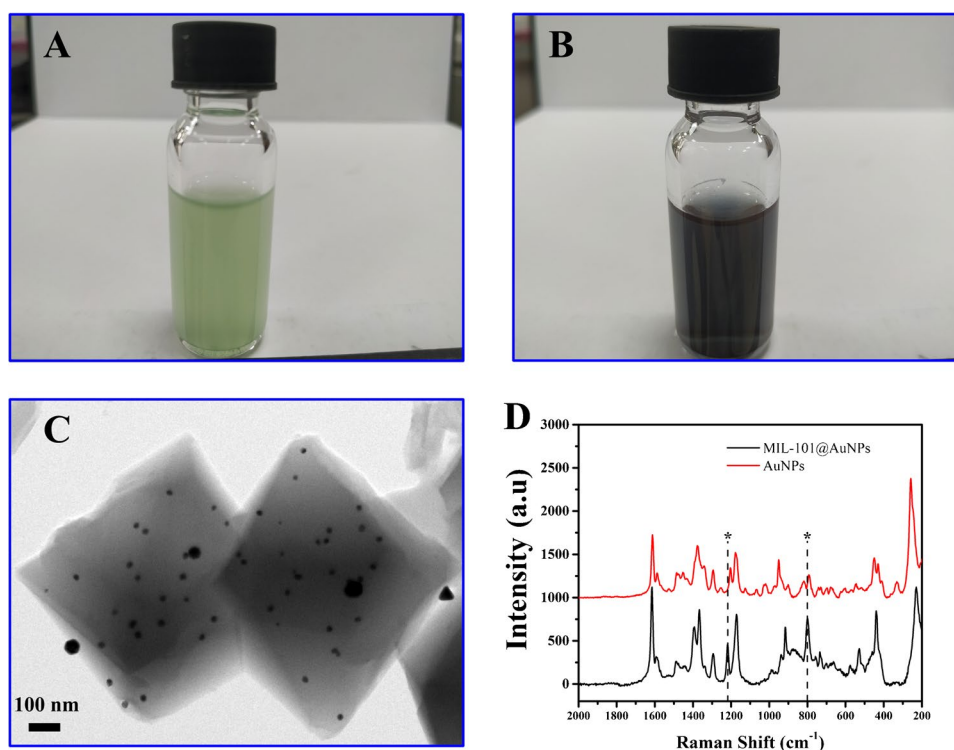
3D materials have been extensively employed in SERS detection owing to their rapid concentration/enrichment effects for target molecules and to the construction of 3D hot spots after assembling of noble metals [20]. However, removing the unwanted impurities in these 3D materials becomes more difficult because of their porosity, allowing for the strong absorption of molecules [43], and therefore,

interfering with SERS detection. Figure 4 illustrates the proposed strategy of photoreduction synthesis of AuNPs in situ assembling in MOF (MIL-101(Cr)) for SERS detection. Figure 4A and B illustrate that the MIL-101(Cr)@AuNPs were well dispersed, and that the color of the g-C₃N₄ aqueous solution turned dark (red shift) after AuNPs assembly. This indicated that the MIL-101(Cr)@AuNPs were successfully prepared, which was verified by TEM (Fig. 4C). Figure 4D illustrates that the Raman shift of MG from MIL-101(Cr)@AuNPs corresponded to AuNPs, except the peak at 1218 cm⁻¹ and 800 cm⁻¹, which corresponded to the MIL-101(Cr) [44]. On the other hand, the SERS signal of MG (1.0×10^{-10} mol/L) was dramatically stronger than that (1.6×10^{-7} mol/L MG) of the AuNPs at 1611 cm⁻¹ of Raman shift. Fig. S11 B compares the SERS signal of the same concentration MG obtained from MIL-101(Cr)@AuNPs and AuNPs. The SERS signal of MG from MIL-101(Cr)@AuNPs was about 45-fold as high as AuNPs, while the SERS signal of MG from MIL-101(Cr)@AuNPs was lower than g-C₃N₄@AuNPs, owing to the π - π and electrostatic interactions of g-C₃N₄ [39].

Evaluation of the proposed strategy

A comparison between the proposed method and other methods for AuNPs synthesis is presented in Table 1S.

Fig. 4 In situ assembling of AuNPs in MIL-101(Cr) and its application for SERS detection. **A** Photographs of MIL-101(Cr) aqueous solution. **B** Photographs of MIL-101(Cr)@AuNPs aqueous solution. **C** TEM of MIL-101@AuNPs. **D** SERS detection of MG with MIL-101(Cr)@AuNPs. 1.6×10^{-7} mol/L of MG for AuNPs; 1.0×10^{-10} mol/L MG for MIL-101(Cr)@AuNPs



The comparison of these methods clearly depicts that the proposed method is simple and more feasible than other reported methods. When in term of the application of AuNPs assembled substrates in different dimension, the sensitivity of the SERS substrates prepared via our proposed methods reached that of most of the previous assays for MG and TBA (Table S2). These results suggest that the proposed strategy have the potential to assemble AuNPs in other materials and to be applied to the fields of catalysis, biology, and materials engineering.

Conclusions

Dispersible AuNPs were synthesized using a simple surfactant-free photochemical method with CH_3OH under UV irradiation. Additionally, the mechanism of AuNPs preparation was investigated. Moreover, this method could directly assemble AuNPs in situ on the multidimensional substrates, and the residual CH_3OH could be easily removed. The present work provides an alternative method for the green synthesis of AuNPs and highlights the potential of this method in preparing other multidimensional SERS substrates. Finally, this synthesis method is expected to have wide applications in sensing, catalysis, and photothermal therapy.

Supplementary Information The online version contains supplementary material available at <https://doi.org/10.1007/s00604-022-05379-2>.

Funding This work was supported by the National Natural Science Foundation of China (Nos. 21964008, 22104025), Guangxi Natural Science Foundation of China (Nos. 2020GXNSFBA159050, 2019GXNSFBA245100, 2020GXNSFBA297147), Guangxi science and technology base and talent special project (No. GuikeAD20238050), and the Students' Platform for Innovation and Entrepreneurship Training Program (No. 202010601022).

Declarations

Conflict of interest The authors declare no competing interests.

References

1. Kneipp J, Kneipp H, Kneipp K (2008) SERS—a single-molecule and nanoscale tool for bioanalytics. *Chem Soc Rev* 37:1052
2. Vega MM, Bonifacio A, Lughini V et al (2014) Long-term stability of surfactant-free gold nanostars. *J Nanopart Res* 16
3. Jadhav K, Hr R, Deshpande S et al (2018) Phytosynthesis of gold nanoparticles: characterization, biocompatibility, and evaluation of its osteoinductive potential for application in implant dentistry. *Mater Sci Eng, C* 93:664–670
4. Yang B, Chou J, Dong X et al (2017) Size-controlled green synthesis of highly stable and uniform small to ultrasmall gold nanoparticles by controlling reaction steps and pH. *The Journal of Physical Chemistry C* 121:8961–8967

5. Prakash A, Pathrose BP, Mathew S et al (2018) Variations in thermo-optical properties of neutral red dye with laser ablated gold nanoparticles. *Opt Mater* 79:237–242
6. Chen C Li Y, Kerman S et al (2018) High spatial resolution nanoslit SERS for single-molecule nucleobase sensing. *Nat Commun* 9
7. Su Y, Shi Y, Wang P et al (2019) Quantification and coupling of the electromagnetic and chemical contributions in surface-enhanced Raman scattering. *Beilstein J Nanotech* 10:549–556
8. Daruich De Souza C, Ribeiro Nogueira B, Rostelato MECM (2019) Review of the methodologies used in the synthesis of gold nanoparticles by chemical reduction. *J Alloy Compd* 798:714–740
9. Jadoun S, Arif R, Jangid NK et al (2021) Green synthesis of nanoparticles using plant extracts: a review. *Environ Chem Lett* 19:355–374
10. Kalimuthu K, Cha BS, Kim S et al (2020) Eco-friendly synthesis and biomedical applications of gold nanoparticles: A review. *Microchem J* 152:104296
11. Nasaruddin RR, Chen T, Yao Q et al (2021) Toward greener synthesis of gold nanomaterials: From biological to biomimetic synthesis. *Coordin Chem Rev* 426:213540
12. El-Borady OM, Ayat MS, Shabrawy MA et al (2020) Green synthesis of gold nanoparticles using Parsley leaves extract and their applications as an alternative catalytic, antioxidant, anticancer, and antibacterial agents. *Adv Powder Technol* 31:4390–4400
13. Naharuddin NZA, Sadrolhosseini AR, Abu Bakar MH et al (2020) Laser ablation synthesis of gold nanoparticles in tetrahydrofuran. *Opt Mater Express* 10:323
14. López-Lorente AI, Simonet BM, Valcárcel M et al (2014) Characterization of stainless steel assisted bare gold nanoparticles and their analytical potential. *Talanta* 118:321–327
15. Kumari G, Kandula J, Narayana C (2015) How far can we probe by SERS? *The Journal of Physical Chemistry C* 119:20057–20064
16. Vesga MJ, Mckechnie D, Laing S et al (2021) Effect of glycine on aggregation of citrate-functionalised gold nanoparticles and SERS measurements *Colloids and surfaces A Physicochemical and engineering aspects* 621:126523
17. Kumari Y, Kaur G, Kumar R et al (2019) Gold nanoparticles: new routes across old boundaries. *Adv Colloid Interfac* 274:102037
18. Wu J, Zhang L, Huang F et al (2020) Surface enhanced Raman scattering substrate for the detection of explosives: construction strategy and dimensional effect. *J Hazard Mater* 387:121714
19. Lai H, Xu F, Zhang Y et al (2018) Recent progress on graphene-based substrates for surface-enhanced Raman scattering applications. *J Mater Chem B* 6:4008–4028
20. Lai H, Li G, Xu F et al (2020) Metal-organic frameworks: opportunities and challenges for surface-enhanced Raman scattering - a review. *J Mater Chem C* 8:2952–2963
21. Harada M, Kizaki S (2016) Formation mechanism of gold nanoparticles synthesized by photoreduction in aqueous ethanol solutions of polymers using in situ quick scanning X-ray absorption fine structure and small-angle X-ray scattering. *Cryst Growth Des* 16:1200–1212
22. Chen Y, Chang W, Lin C (2021) Selective growth of patterned monolayer gold nanoparticles on SU-8 through photoreduction for plasmonic applications. *ACS Appl Nano Mater* 4:229–235
23. Yang S, Zhou L, Su Y et al (2019) One-pot photoreduction to prepare NIR-absorbing plasmonic gold nanoparticles tethered by amphiphilic polypeptide copolymer for synergistic photothermal-chemotherapy. *Chinese Chem Lett* 30:187–191
24. Mihály M, Fleancu MC, Olteanu NL et al (2012) Synthesis of gold nanoparticles by microemulsion assisted photoreduction method. *Cr Chim* 15:1012–1021
25. Kwolek P, Wojnicki M (2014) The kinetic study of photoreduction of tetrachloroaurate acid by methanol in acidic media. *J Photochem Photobiol, A* 286:47–54
26. Tian J, Liu Q, Ge C et al (2013) Ultrathin graphitic carbon nitride nanosheets: a low-cost, green, and highly efficient electrocatalyst toward the reduction of hydrogen peroxide and its glucose biosensing application. *Nanoscale* 5:8921
27. Su L, Xiong Y, Yang H et al (2016) Prussian blue nanoparticles encapsulated inside a metal–organic framework via in situ growth as promising peroxidase mimetics for enzyme inhibitor screening. *J Mater Chem B* 4:128–134
28. Mirkhalaf F, Paprotny J, Schiffrin DJ (2006) Synthesis of metal nanoparticles stabilized by metal–carbon bonds. *J Am Chem Soc* 128:7400–7401
29. Jain PK, Huang W, El-Sayed MA (2007) On the universal scaling behavior of the distance decay of plasmon coupling in metal nanoparticle pairs: a plasmon ruler equation. *Nano Lett* 7:2080–2088
30. Unal IS, Demirbas A, Onal I et al (2020) One step preparation of stable gold nanoparticle using red cabbage extracts under UV light and its catalytic activity. *J Photochem Photobiol, B* 204:111800
31. Shiraishi Y, Tanaka H, Sakamoto H et al (2017) Synthesis of Au nanoparticles with benzoic acid as reductant and surface stabilizer promoted solely by UV light. *Langmuir* 33:13797–13804
32. Ashley B, Vakil PN, Lynch BB et al (2017) Microwave enhancement of autocatalytic growth of nanometals. *ACS Nano* 11:9957–9967
33. Harada M, Einaga H (2007) In situ XAFS studies of Au particle formation by photoreduction in polymer solutions. *Langmuir* 23:6536–6543
34. Baffou G, Quidant R, García De Abajo FJ (2010) Nanoscale control of optical heating in complex plasmonic systems. *ACS Nano* 4:709–716
35. Mitomo H, Horie K, Matsuo Y et al (2016) Active gap SERS for the sensitive detection of biomacromolecules with plasmonic nanostructures on hydrogels. *Adv Opt Mater* 4:259–263
36. Hu B, Pu H, Sun D (2021) Multifunctional cellulose based substrates for SERS smart sensing: Principles, applications and emerging trends for food safety detection. *Trends Food Sci Tech* 110:304–320
37. Kim EJ, Kim H, Park E et al (2021) Paper-based multiplex surface-enhanced raman scattering detection using polymerase chain reaction probe codification. *Anal Chem* 93:3677–3685
38. Jiang J Zou S, Li Y et al (2019) Flexible and adhesive tape decorated with silver nanorods for in-situ analysis of pesticides residues and colorants. *Microchim Acta* 186
39. Qu L, Wang N, Xu H et al (2017) Gold nanoparticles and g-C₃N₄-intercalated graphene oxide membrane for recyclable surface enhanced Raman scattering. *Adv Funct Mater* 27:1701714
40. Huang X Zeng Z, Bao S et al (2013) Solution-phase epitaxial growth of noble metal nanostructures on dispersible single-layer molybdenum disulfide nanosheets. *Nat Commun* 4
41. Panimalar S, Uthrakumar R, Selvi ET et al (2020) Studies of MnO₂/g-C₃N₄ hetrostructure efficient of visible light photocatalyst for pollutants degradation by sol-gel technique. *Surfaces and Interfaces* 20:100512
42. Yang S, Dai X, Stogin BB et al (2016) Ultrasensitive surface-enhanced Raman scattering detection in common fluids. *Proc Natl Acad Sci* 113:268–273
43. Jiang X, Ruan G, Deng H et al (2021) Synthesis of amphiphilic and porous copolymers through polymerization of high internal phase carboxylic carbon nanotubes emulsions and application as adsorbents for triazine herbicides analysis. *Chem Eng J* 415:129005
44. Al Lafi AG Assfour B, Assaad T(2020) Metal organic framework MIL-101(Cr) spectroscopic investigations to reveal iodine capture mechanism. *J Inorg Organomet* 30 1218–1230

Publisher's note Springer Nature remains neutral with regard to jurisdictional claims in published maps and institutional affiliations.